Received: 24 February 2022 | Revised: 27 July 2022 | Accepted: 19 August 2022

DOI: 10.1111/ffe.13829

ORIGINAL ARTICLE

FFEMS Fatigue & Fracture of Engineering Materials & Structures WILEY

Experiments and numerical simulations on dynamic crack behavior at the interface of layered brittle material

Jun Zhou[1] | **Zhongwen Yue**[1,2] | **Chun Feng**[3] | **Peng Wang**[1] | **Xiaolei Yue**[1] | **Tiejun Tao**[4]

[1]School of Mechanics & Civil Engineering, China University of Mining and Technology (Beijing), Beijing, China

[2]Institute of Modern Blasting Technology Application, China University of Mining and Technology (Beijing), Beijing, China

[3]Key Laboratory for Mechanics in Fluid Solid Coupling Systems, Institute of Mechanics, Chinese Academy of Sciences, Beijing, China

[4]School of Civil Engineering, Guizhou University, Guiyang, China

Correspondence
Zhongwen Yue, School of Mechanics & Civil Engineering, China University of Mining and Technology (Beijing), Beijing, 100083, China.
Email: zwyue75@163.com

Funding information
National Natural Science Foundation of China, Grant/Award Number: 52174094

Abstract

Crack behavior at the interface between two materials is the core problem of layered material fracturing. In this paper, first, experimental tests were conducted on layered material using a drop weight test system following the caustics method. The layered material was made of poly (methyl methacrylate) (PMMA) and epoxy resin bonded with Loctite-330 at two inclination angles (30° and 60°). A corresponding numerical simulation was carried out using continuum–discontinuum element methods. Crack propagation is found to mainly occur in mode I in the PMMA and epoxy resin but follows a mixed cracking mode at the interface. The fracture parameters of the crack tip in the layered materials changed substantially owing to the existence and change of the interface structure. After the crack enters the interface, the crack propagation speed increases significantly. Higher crack dip angles are associated with greater crack propagation speed increases after entering the interface. The simulation results indicate that the interface strength properties affect crack behavior at the interface. This effect also varies as a function of interface inclination and impact velocity.

KEYWORDS

caustics, continuum–discontinuum element method, drop weight tests, interface crack

1 | INTRODUCTION

Engineering structures or natural materials are usually made of different media (layered material). Fractures in layered brittle materials are one of the most general features that must be taken into account in solid mechanics.[1,2] Failure behavior and the deformation of brittle material are strongly affected by the presence of layers[3,4]; crack behavior in such layered brittle materials must therefore be well investigated.

Crack penetration and branching are controlled by the material properties, which depend on the thickness and stiffness of the layers and the layer inclination angles between the loading direction and bedding plane.[5–7]

Numerous experimental studies have investigated the fracturing behavior of layered brittle material using a variety of methods. For example, Heng et al.[8] investigated the effect of interface orientation on the shear fracturing of shale based on direct shear tests. Their study indicated that the anisotropy of shear failure is determined by the interface orientation and normal stress of the shale. The properties of the interface are affected by the cohesive strength and friction. Ma et al.[9] proposed a fracture pressure model to investigate the anisotropy of tensile failure in layered brittle materials and showed that the strength of layered brittle materials increases with the loading angle. Dynamic photoelasticity was well applied by Chalivendra and Rosakis[10] to observe real-time optical parameters associated with crack propagation. Liu et al.[11] applied an electromagnetic impact setup to study dynamic interlaminar crack propagation via mode I in composite material. Yan et al.[12] tested the dynamic interface tensile strength between tuff and basalt using a SHPB impact system and showed that the impact loading rate has a notable effect on the dynamic tensile strength of the interface. Sundaram and Tippur[13] introduced digital gradient sensing to evaluate the dynamic fracture behavior of layered architecture containing crack penetration, trapping, and branching at an interface. Alneasan et al.[14] investigated the interface crack problem of dissimilar layered rock and analyzed the effect of crack inclination angle on the fracture parameters and mechanic characteristics of the interface crack tip. Qiu et al.[15] used the SMCT specimen to investigate the crack behavior of mortar–rock interfaces and determined the effect of loading rate and interface roughness on the interface crack. Layered rock is a common brittle material in engineering; the effect of layering on the measured peak strength, deformation, and fracture behavior of the rock has been well researched.[16–19] However, because rock is an opaque material, transparent brittle materials are widely used to replace rock to investigate brittle fracture problems, for which it is easier to obtain fracture parameters using optical experimental methods.[20–24]

Appropriate numerical simulations are an alternative tool to obtain useful insight on the stress distribution and fracture behavior and to interpret laboratory test results. The prediction of crack initiation, propagation, and crack path into brittle material is a fundamental problem in fracture mechanics. An accurate numerical model of these problems is therefore of great importance in fracture mechanics. The mechanical response and fracture characteristic of layered brittle materials have been previously simulated using a variety of numerical methods (e.g., continuous method and discontinuous method).[25–30] The strength, deformation, and failure behavior of layered brittle materials and the tensile fracture and shear fracture along bedding planes have been well simulated. Recently, to accurately reproduce the progressive damage and failure evolution of material from a continuous to a discontinuous state, the coupled method (e.g., finite-discrete element method, FDEM) has been applied to capture the failure process of layered material, which combines advantages of both continuous and discontinuous approaches.[31,32] For example, Sun et al.[33] applied the FDEM to investigate the thermal cracking process in anisotropic rock formations; and material anisotropy, preexisting discontinuities, and multiple layers are simulated well in their model. Chen and Chan[34] applied the FDEM to simulate the fracture response of the interlayer of laminated glass and demonstrated the advantage of the FDEM for modeling fracturing in laminated glass. Ju et al.[35] used the continuum–discontinuum element method (CDEM) to model multilayered heterogeneous rock strata in underground projects. Their study indicated that the CDEM combines the effectiveness of FEM in mining-induced stress solutions with the accuracy of DEM results for handling the initiation and propagation of fractures in multilayered rock mass. Conventionally, the CDEM couples finite element calculations with discrete element calculations. It conducts finite element calculations inside the block elements and conducts discrete element calculations at the block element boundaries, which is different from the domain decomposition methodology. Based on CDEM, the deformation and force of a structure can be accurately calculated via the continuous element method. The interaction between adjacent blocks can be transmitted by a contact element.

For the delamination analysis of laminated composites, there are also many valuable research work.[36,37] For example, Alfano and Crisfield applied the finite element analysis to discuss the issues related with the numerical solution of the non-linear problem of the delamination.[38] Torabi and Pirhadi proposed a newly concept, called the Virtual Isotropic Material Concept (VIMC), accompanying with two well-known brittle failure models, to predict the theoretical LPF load under mixed mode I/II loading.[39] Numerous studies have addressed the brittle fracture behavior of interfaces in layered material, including theoretical analysis, numerical simulations, and experimental studies.[40–44] The effect of mismatching elastic moduli of the host materials on the interface cracking, macroscopic deformation, and failure characteristics are the main factors considered in these studies. Micro-fracture parameters of the moving crack in layered materials and the effect of interface strength properties on the interface crack behavior require further study. Therefore, this paper using high-speed photography to investigate the fracture parameters of crack tips in layered materials following the caustics method. A numerical model for interface cracking was also developed by implementing the mixed-mode failure criterion in the CDEM. The accuracy of the numerical model is verified by the experimental results. Although many papers in the existing literature already addressed this subject with very similar experimental or numerical approaches,[44,45] there are relatively few systematic studies on the influence of the mechanical properties and structural characteristics of the interface on layered materials. In addition, the numerical calculation in this paper not only makes use of the computational advantages of CDEM in crack problems but also introduces the theoretical calculation formula of spring stiffness into the

CDEM calculation framework for the first time, which solves the disadvantages of the empirical value of spring stiffness in traditional CDEM and FDEM.

2 | EXPERIMENTAL STUDY

2.1 | Sample preparation

Experimental tests for layered materials (poly (methyl methacrylate) (PMMA)/epoxy resin) were carried out using the combined caustic method and drop weight experimental system. Two loading angles ($\omega = 30°$, $60°$) are considered in this work, which are defined as the angle between the loading direction and the material interface. To create a strong interface, the interface between the PMMA and epoxy resin was bonded using Loctite-330 adhesive. For the adhesive, the adopted values were Young's modulus = 800 MPa, Poisson's ratio = 0.15, shear strength = 20.2 MPa, tensile strength = 35 MPa, mode I fracture energy = 0.12 N/mm, and mode II fracture energy = 0.24 N/mm.[46] Additional surface preparation was performed prior to bonding to obtain an effective bonding surface of the two layers. Sandpaper was first used to polish the surface of the specimen to be bonded to maintain bonding surface flat, and then cleaned of any residue on the surface. Before using the adhesive, the activator was spread evenly on the two bonding surfaces. Specimens were allowed to cure for 48 h prior to the experiment.

As shown in Figure 1, the overall dimensions of the specimens are 220 × 50 × 5 mm (width × height × thickness). A pre-existing notch of 5 mm in length and 0.8 mm in width is perpendicularly set at the edge of the specimen. The notch tip is sharpened by a diamond wire saw to guarantee a typical mode I cracking path under the impact load. The materials A and B are epoxy resin and PMMA, respectively. Three specimens were tested for each configuration.

2.2 | Test apparatus

The dynamic fracture behavior of materials is different from the static fracture behavior. The dynamic fracture strength of materials is often related to the dynamic loading rate. Therefore, the dynamic crack behavior of materials is different under different loading rates. This study used a dynamic loading system based on a three-point bend testing apparatus combined with a drop weight. In the drop weight test system, the impact energy is produced by the free fall of a hammer from a certain height. The impact velocity of the drop weight can therefore be controlled by designing the drop height. In this

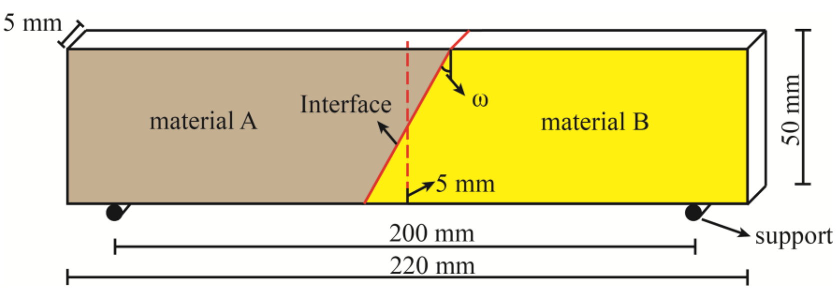

FIGURE 1 Schematic diagram of a layered specimen loaded in three-point bending by a drop weight impact system [Colour figure can be viewed at wileyonlinelibrary.com]

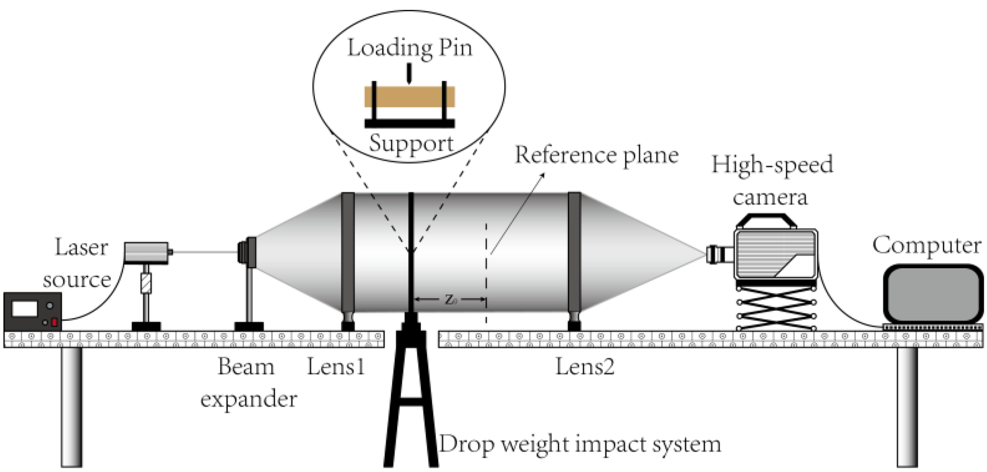

FIGURE 2 Schematic diagram of the dynamic caustics experimental system [Colour figure can be viewed at wileyonlinelibrary.com]

experimental test, the weight of the hammer was 1.2 kg. The setup of the dynamic caustics experimental system is shown in Figure 2, including a high-speed camera (Fastcam-SA5-16G, Photron Co., Japan) used for data recording. To achieve accurate data acquisition, it is necessary to ensure that the surface of the layered specimen remains perpendicular to the parallel light beam. The length between the imaging plane of the camera and the specimen middle plane is 300 cm, which is represented by the symbol Z_0 in classical caustics theory.[47] The recording speed of camera is 100,000 frames per second, and a resolution of 320 × 192 pixels is used in the photography.

2.3 | Fracture parameters measurement

The caustics method was developed combining high-speed photography with optical theory of materials.[48] When a crack occurs in a transparent material in the beam, the thickness of the material around the crack tip changes. The light beam previously transmitted in parallel deflects around the crack tip, and a shadow spot around the crack tip occurs at some distance behind the specimen. There is an inherent relationship between these optical parameters and the stress state at the crack tip. The principle of caustics method is to establish the quantitative theoretical formula for this relationship. Thus, the fracture parameters of the moving crack tip can be determined by the caustics method.[23] In this method, stress intensity factors (SIFs) can be obtained:

$$K_I = \frac{2\sqrt{2}\pi}{3Z_0 d c_t \lambda^{3/2}} \left(\frac{D_{T,L}}{\delta_{T,L}}\right) f(v) \tag{1}$$

$$K_{II} = \mu K_I \tag{2}$$

where $D_{T,L}$ represents the maximum diameter of the caustic pattern and $\delta_{T,L}$ is a coefficient related to $D_{T,L}$, the values of them are 3.1702 and 3, respectively. Terms d, c_t, and λ denote the specimen thickness, stress optical constant, and scale factor, respectively. The value of them are 0.005 m, $0.85 \times 10^{-10}\,\mathrm{m^2/N}$ and 1, respectively. $f(v)$ is the dynamic correction factor considering crack velocity, but change of caustics geometry due to crack velocity can be ignored. The ratio of DT/DL increases with crack velocity; however, this increase is very small, below 0.4% at 400 m/s[20]. Thus, in most cases, change of caustics geometry due to crack velocity can be ignored. μ is a coefficient related to $(D_{L\max} - D_{L\min})/D_{L\max}$,[20] $D_{L\max}$ and $D_{L\min}$ are the maximum longitudinal diameter and

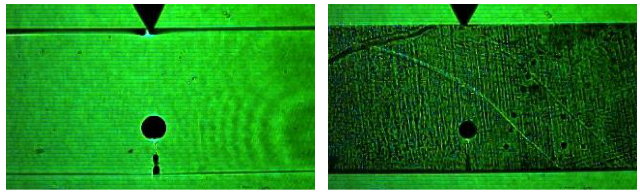

(A) PMMA (B) Epoxy

FIGURE 3 (A and B) Caustic image patterns of the two materials under drop weight loading [Colour figure can be viewed at wileyonlinelibrary.com]

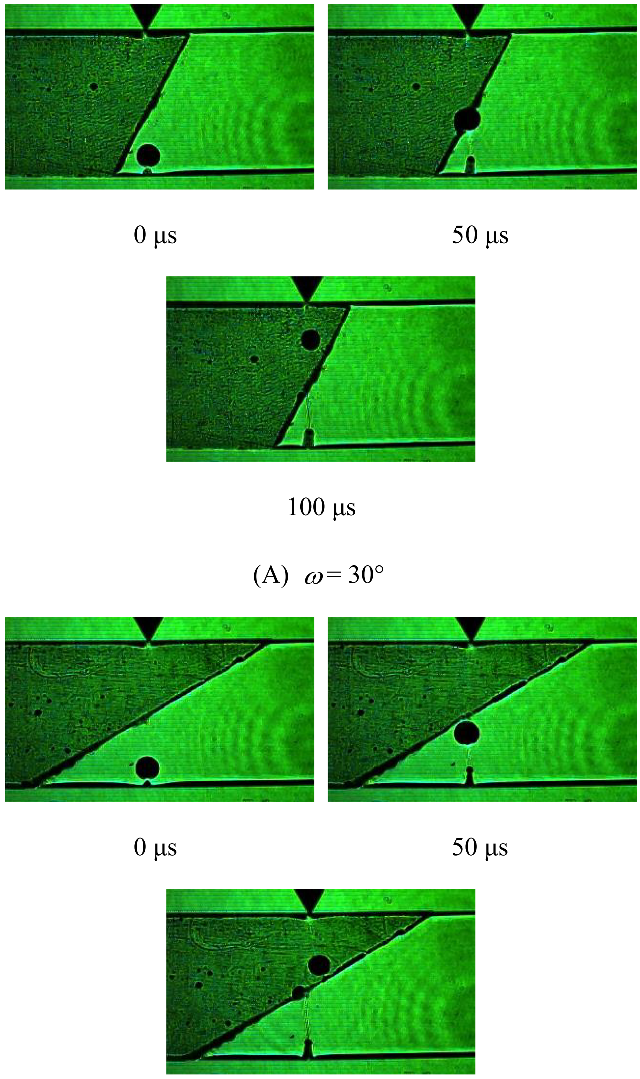

0 µs 50 µs

100 µs

(A) $\omega = 30°$

0 µs 50 µs

100 µs

(B) $\omega = 60°$

FIGURE 4 (A and B) Caustic image patterns of layered specimen for two loading angles [Colour figure can be viewed at wileyonlinelibrary.com] the minimum longitudinal diameter of the asymmetrical caustics pattern, respectively.

Typical caustic images of the different monolithic specimens under drop weight loading are shown in Figure 3. The impact point is located on the centerline of the specimen to ensure mode I loading conditions. The calculated values of the initial stress intensity factors of PMMA and epoxy are 1.1 and 0.68 $MPa{\cdot}m^{1/2}$, respectively.

2.4 | Effect of loading angle on the fracture characteristics of the interfacial crack

Figure 4 shows typical caustic spots of the specimens with two loading angles. The mode I moving crack tip in the PMMA material can be identified by the caustic shadow spot until it approaches the interface. The shadow spot of the interface of the moving crack corresponding to the PMMA is small, and the asymmetry in the shadow spot patterns of the interface cracks indicates mixed-mode cracking in the interface. The initial mode I crack propagates in the PMMA medium before approaching the interface. When approaching the interface, the propagation of the crack deflects along the interface for a distance, then emerges from the interface into the epoxy resin. Figure 5 shows that the travel distance of the moving crack in the interface is reduced from 12 to 6 mm upon increasing the loading angle from 30° to 60°. The final crack propagation path pattern in the layered specimen is shown in Figure 5. There are only marginal differences for identical loading angles.

Figure 6 shows plots of the stress intensity factors in the two configurations. It is noted that $t = 0$ μs appears to be the time of crack initiation at the pre-cut notch. Figure 6A shows the stress intensity factor histories of

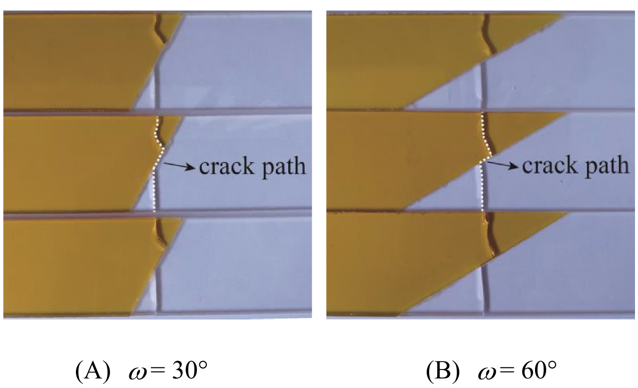

FIGURE 5 (A and B) Experiment repeatability [Colour figure can be viewed at wileyonlinelibrary.com]

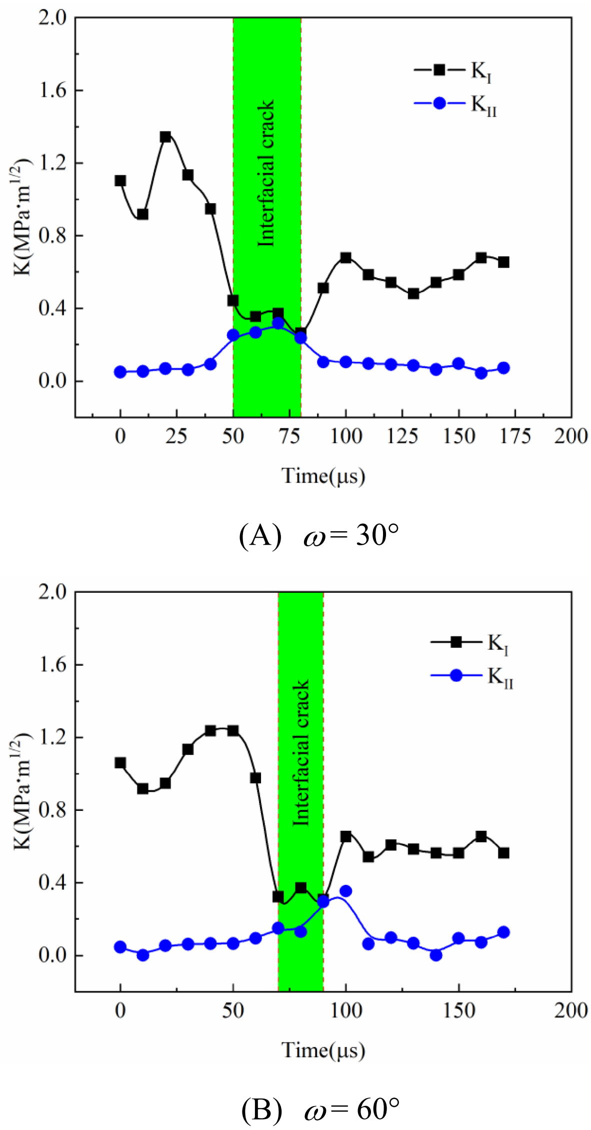

FIGURE 6 (A and B) Evolution of stress intensity factors in the two configurations [Colour figure can be viewed at wileyonlinelibrary.com]

the propagating crack in the case of a 30° loading angle. The change curve of the stress intensity factor initially decreases and then increases. Before the crack reaches the interface, K_I increases to a peak value of 1.34 $MPa{\cdot}m^{1/2}$, while the value of K_{II} remains nearly zero in the PMMA material. As the crack reaches the interface, K_I decreases rapidly. When crack enters the interface from PMMA, K_{II} increases prominently, suggesting a mixed-mode crack in the interface. When cracks penetrate epoxy resin material, K_{II} again approaches zero. Figure 6B shows the stress intensity factor histories of a specimen in the case of a 60° loading angle. The sample with the 60° loading angle also shows similar distinct characteristics. Before the crack approaches the interface, K_I reaches a peak value of 1.24 $MPa{\cdot}m^{1/2}$, which is lower than that in the case of the 30° loading angle. Figure 7 shows the evolution of the velocity histories of the moving crack tip in both specimen configurations. Four distinct regions can be identified in the crack velocity histories of the bi-material specimens. In region I, the velocity of the initiating crack gradually reaches a constant level for propagation. A reduction of crack-tip velocity is found in both configurations near the interface. In region II, the interface crack velocity increases rapidly, and the measured crack velocity is considerably higher in the case of the 30° loading angle. In region III, a rapid velocity decrease occurs in both cases and remains a constant value for a period of time. In region IV, the crack velocities are much lower in the vicinity of the loading pin.

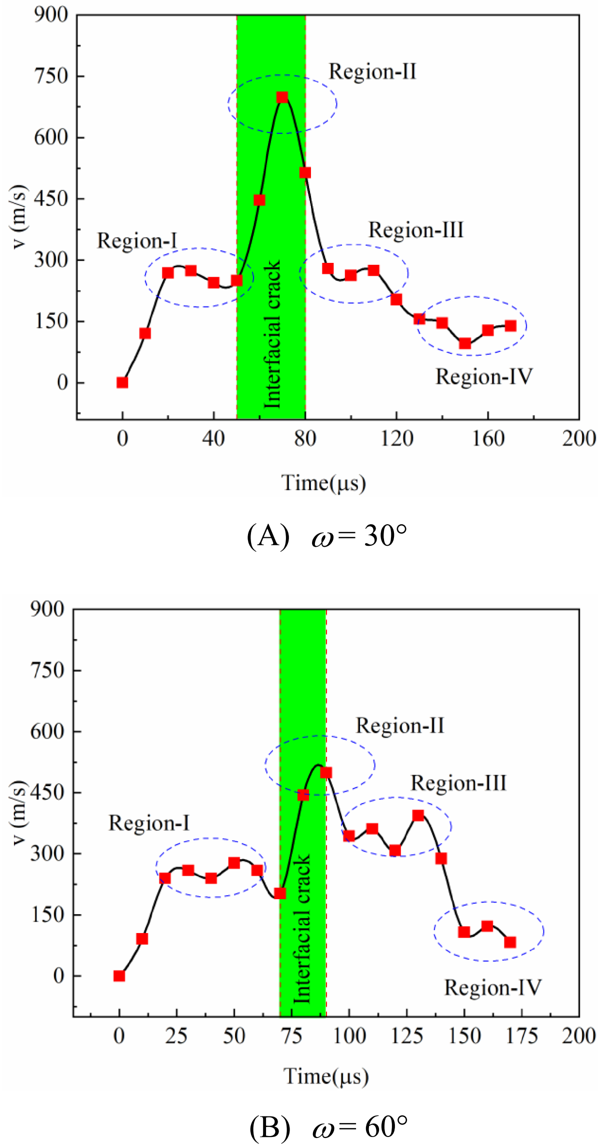

FIGURE 7 (A and B) Crack velocity histories of the two configurations [Colour figure can be viewed at wileyonlinelibrary.com]

3 | NUMERICAL STUDY

3.1 | Computational model description

The computational domain can be discretized into finite elements, which can be partially continuous, that is, CDEM domains.[49] The CDEM domain can be used to simulate the evolution of block elements from a continuous to a discontinuous field by constructing contact interfaces between adjacent blocks.[50] As shown in Figure 8, the discrete domain is created along the anticipated crack path, and the remaining part is set as the continuous domain. This greatly reduces the required computation time because the discretization of the entire numerical model is avoided.

The failure mechanism between the two blocks is interpreted by springs, which connect the FE and DE elements. A stress-based, mixed-mode failure criterion is implemented into the traditional CDEM framework to accurately simulate interface cracking.[51] The maximum tensile-stress criterion and mixed-mode failure criterion are applied to investigate the failure evolution of the host material and the interface, respectively:

$$\text{Tensile failure criterion}: \sigma_T \geq -\sigma_T \tag{3}$$

$$\begin{gathered}\text{Mixed-mode failure criterion}^{36}: \\ \left(\max\left(0, \sigma_T\right)/\overline{\sigma}_{TI}\right)^2 + \left(\sigma_S/\overline{\sigma}_{SI}\right)^2 = 1\end{gathered} \tag{4}$$

where $\overline{\sigma}_T$ is the tensile strength of the host material, σ_T and σ_S are the normal and shear stresses in the current time step, respectively, and $\overline{\sigma}_{TI}$ and $\overline{\sigma}_{SI}$ are the tensile and shear strength of the interface, respectively, which is defined by the strength of the adhesive. This can be calculated from the stiffness value based on the theory of material strength in molecular mechanics and material fracturing as[52]

$$\begin{cases} k_n = \dfrac{E\overline{\sigma}_T}{4G_f^I} \\ k_s = \dfrac{G\overline{\sigma}_T}{4G_f^{II}} \\ G = \dfrac{E}{2(1+\nu)} \end{cases} \tag{5}$$

where k_n, k_s, G_f^I, G_f^{II}, E, G, ν, and $\overline{\sigma}_T$ are the normal stiffness, shear stiffness, mode I fracture energy, mode II

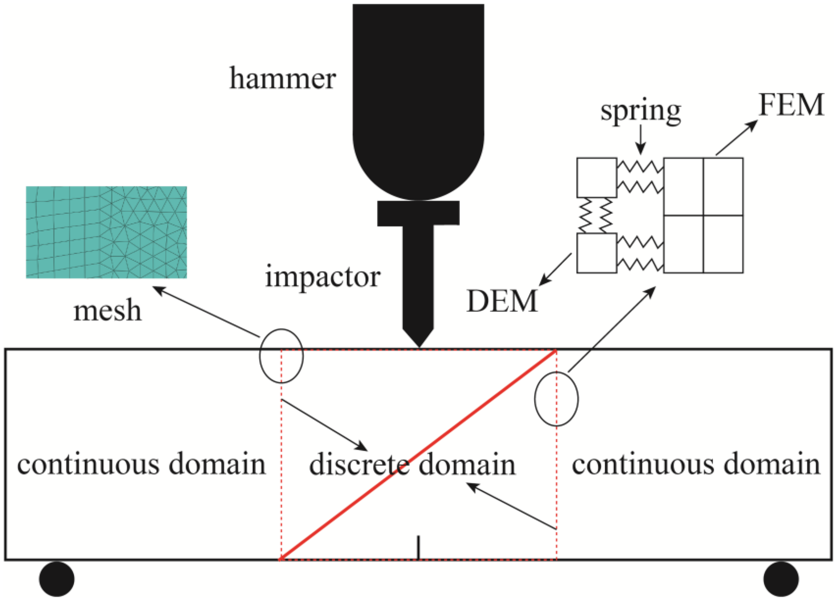

FIGURE 8 Numerical model of the drop weight system [Colour figure can be viewed at wileyonlinelibrary.com]

TABLE 1 Mechanical properties of the layered material

Material	E(GPa)	υ	ρ(kg/m^3)	σ_t(MPa)
PMMA[54]	6.1	0.31	1,180	38
Epoxy[55]	3.2	0.35	1,180	37.9

Note: $E =$ elastic modulus; $\upsilon =$ Poisson's ratio; $\sigma_t =$ tensile strength; $\rho =$ density.

fracture energy, Young's modulus, shear modulus, Poisson's ratio, and tensile strength, respectively. The procedure of the explicit scheme for the CDEM is not presented here; interested readers are referred to Yue et al[53] for a recent overview.

3.2 | Validation of numerical model

A 3D numerical model is established according to the real configuration of the experimental system, which contains a tetrahedron, wedge, and hexahedron elements. The mechanical properties of the host materials used in the experiments are listed in Table 1.

To invest the effect of different finite element dimensions on the numerically predicted crack path, firstly, we need perform a mesh size sensitivity analysis for numerical model. Different finite element size $h = 1$, 1.1, 1.2, 1.3, 1.4 mm around the potential crack path are used in five numerical models for the loading angle 60° case. The effect of element size on the interface crack length is shown in Figure 9. It is found that the length of interface crack in the simulations with mesh sizes of 1 to 1.3 mm is similar. While in the simulations with larger

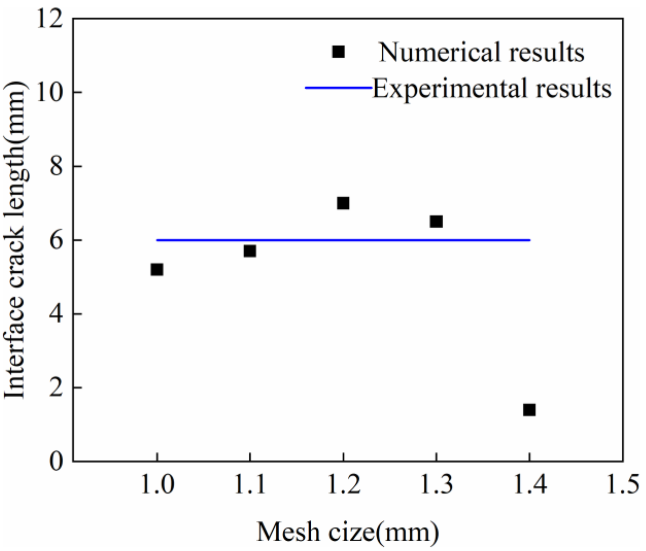

FIGURE 9 Size effect on failure process for the interface fracture of layered materials [Colour figure can be viewed at wileyonlinelibrary.com]

mesh sizes the fracture is significantly different from those in the simulations with smaller mesh sizes. Therefore, it is evident that the crack path converges with the decrease of element size. The case of loading angle 60° is simulated using the proposed numerical model to verify its accuracy. In addition, the mesh topology of the numerical model is shown in Figure 10A, and the finite element size $h = 1$ mm around the potential crack path are used in these numerical models.

The simulation results are shown in Figure 10B,C. The interfacial crack length in the specimens with

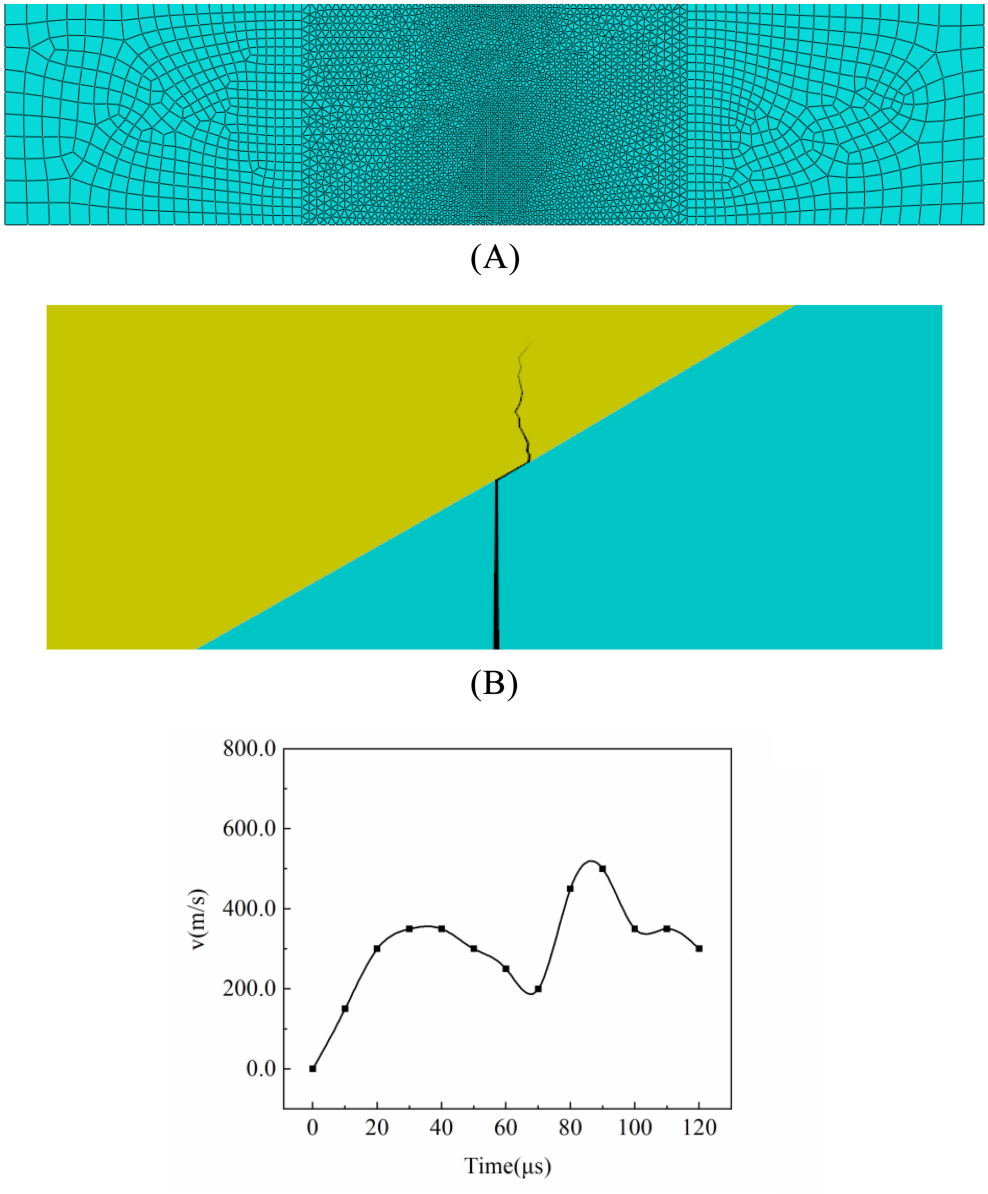

FIGURE 10 Experimental results simulation for (A) mesh topology, (B) crack path, and (C) crack velocity history [Colour figure can be viewed at wileyonlinelibrary.com]

loading angles of 30° and 60° are 11.8 and 5.2 mm, respectively. The simulated crack length shows little difference with that of the experimental values, especially in the case of the 60° loading angle. The crack propagation path calculated by the numerical method is generally consistent with the experimental results, and can successfully simulate the effect of the loading angle on the crack path to a certain extent. This indicates that the proposed model can reasonably simulate the interface crack of layered materials in drop weight experiments. To further verify the numerical model, the numerical simulation of crack velocity histories for the loading case 60° is shown in Figure 10C, and the overall change law is consistent with the experimental results. However, the crack velocity in numerical calculations is higher than that in experiments. There may be two reasons for this error: the first is the error of experimental data measurement (shortcomings of caustic method); Second, in numerical simulation, the calculation parameters of materials are obtained by directly quoting the experimental data in others' articles, rather than from laboratory tests.

3.3 | Effect of interface strength properties on the interface crack of layered materials

The interface fracture characteristics of layered materials are largely determined by the strength parameters (tensile strength and shear strength) of the interfacial

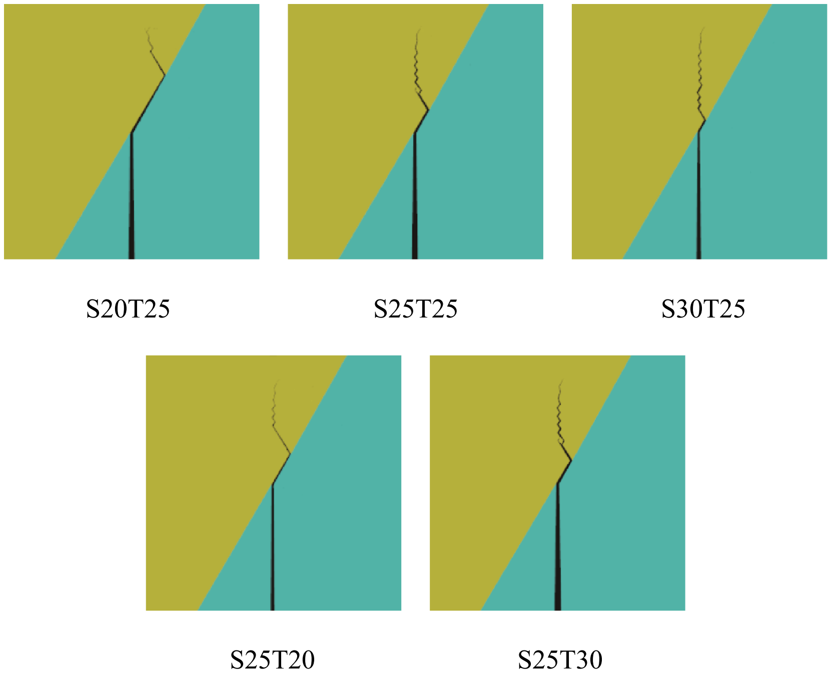

FIGURE 11 Fracture of layered materials in configuration I (S: shear strength; T: tensile strength) [Colour figure can be viewed at wileyonlinelibrary.com]

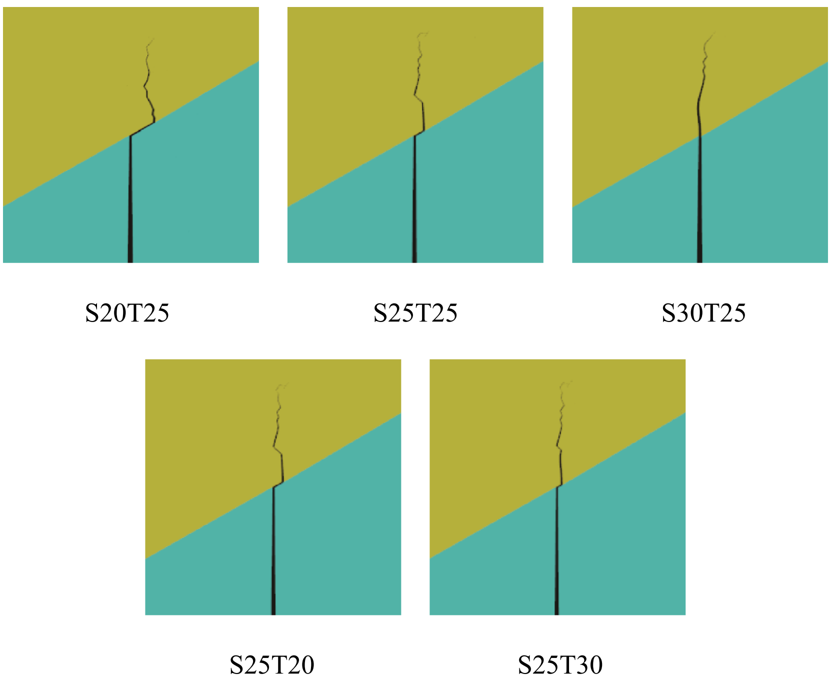

FIGURE 12 Fracture of layered materials in configuration II (S: shear strength; T: tensile strength) [Colour figure can be viewed at wileyonlinelibrary.com]

bonding materials. Numerical test schemes that consider different interface tensile strength and shear strength are designed to investigate the effect of adhesive strength on interface fracturing in the above two experimental configurations. The simulation results are shown in Figures 11 and 12. The numerical simulation results in Figure 11 show that for a loading angle of 30°, the original crack first vertically penetrates the PMMA material and then extends a certain distance at the interface, ultimately entering the epoxy resin. Upon increasing the loading angle to 60°, when the interface strength increases to a certain value (S30T25), the original propagating crack in the PMMA directly passes through the interface into the epoxy resin rather than extending along the interface (Figure 12). The crack propagation distance at the interface generally decreases with increasing interface strength. This shows that the interface property, similar to the interface loading angle, is an important factor that affects the fracture characteristics of the interface. To more directly show the numerical calculation results, Figure 13 compares the interface crack length of the two loading angles. In both configurations, the influence of the interface shear strength on the interface crack propagation is greater than that of the interface tensile strength. The effect of shear strength on the interface crack propagation gradually decreases with increasing loading angle, whereas the interface tensile strength has almost no effect.

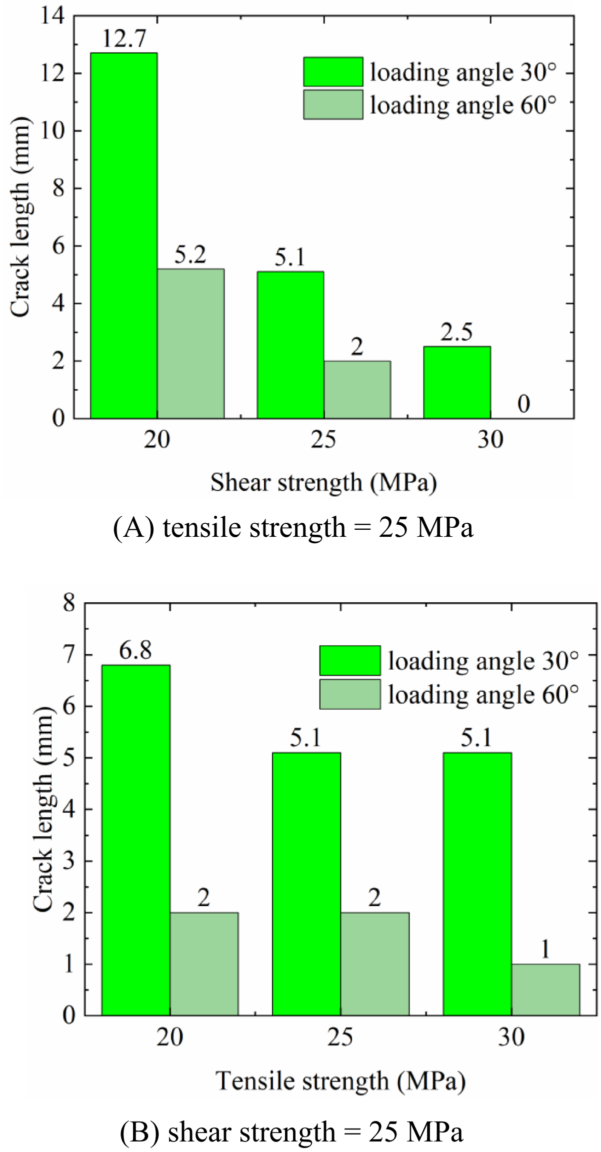

FIGURE 13 Interface crack length in the two configurations at constant (A) tensile strength and (B) shear strength [Colour figure can be viewed at wileyonlinelibrary.com]

3.4 | Effect of impact velocity on the interface crack of layered materials

Three drop hammer impact velocities (1.5, 2.0, and 2.5 m/s) are selected in the numerical model to study its effect on the crack propagation law of interface fracturing. Here, only the configuration with a loading angle of 30° is considered, and the shear strength and tensile strength of the interface are taken as 25 MPa. The numerical results are shown in Figure 14, indicating that the propagation length of the interfacial crack increases significantly with increasing velocity.

Corresponding numerical models are established to further investigate the effect of adhesive strength on the interface crack behavior at different impact velocities. The calculation results of the numerical models are displayed in Figure 15 and show that shear strength has a more notable effect than tensile strength on crack behavior at the interface at an impact velocity of 1.5 m/s. However, with increasing impact velocity, the effect of tensile strength on the interface crack gradually increases.

4 | LIMITATIONS AND FUTURE STUDIES

Although the fracture characteristics and crack behaviors of layered brittle materials is well investigated, there are several limitations in the present work. The experimental results indicate that the measurement of caustics patterns is affected by the adhesive, in particular, the profile of the caustics pattern becomes unclear when the crack tip approaches to the interface. For the numerical method, due to the inherent shortcoming of CDEM, crack

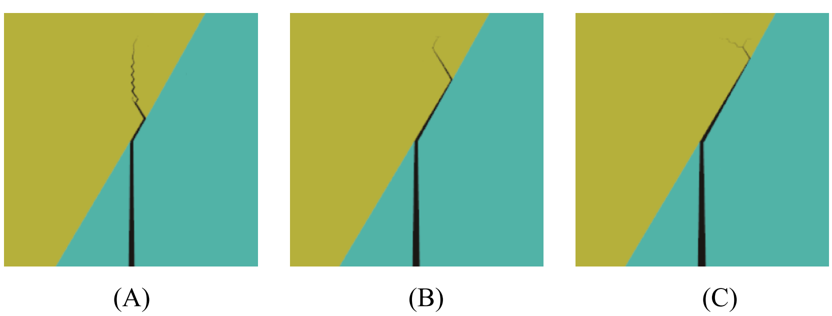

FIGURE 14 Interface fractures developed under different impact velocities: (A) 1.5, (B) 2.0, and (C) 2.5 m/s [Colour figure can be viewed at wileyonlinelibrary.com]

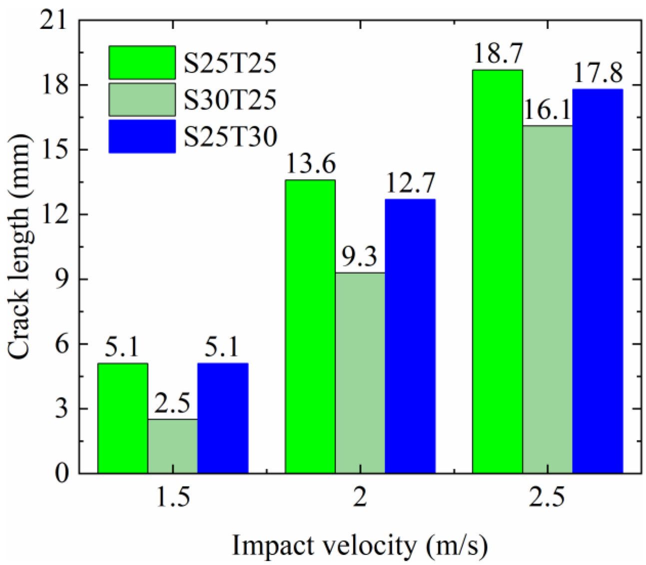

FIGURE 15 Interface crack length for different impact velocities [Colour figure can be viewed at wileyonlinelibrary.com]

calculation is sensitive to the topology of the primary mesh. Further improvements are therefore underway to address these shortcomings.

5 | CONCLUSIONS

This paper presents experiments and simulations on the fracture behavior of interface cracks using a drop weight loading system. The fracture parameters of the propagating crack are obtained by caustics analysis. The effect of strength properties on interface crack behavior are investigated using the CDEM. The main conclusions are as follows.

1. The crack mainly propagates in mode I in the host material (PMMA and epoxy resin) but enters the interface in a mixed mode.
2. After the crack enters the interface, the crack propagation speed increases significantly. Higher crack dip angles are associated with greater crack propagation speed increases after entering the interface.
3. Interface strength has a notable effect on interfacial crack propagation. The effect of shear strength on the interface fracture is greater than that of tensile strength. With increasing interface inclination angle, the effect of shear strength on the interface crack propagation is more notable than that of tensile strength.
4. The propagation length of the interface crack increases significantly with increasing impact velocity. The effect of shear strength on the interfacial crack propagation length gradually decreases with increasing impact velocity, while the effect of tensile strength gradually increases.

ACKNOWLEDGEMENTS

This research was supported by the National Natural Science Foundation of China (No. 52174094).

AUTHOR CONTRIBUTIONS

Jun Zhou: Conceptualization, methodology, investigation, formal analysis, visualization, data curation, and writing–original draft. **Zhongwen Yue:** Funding acquisition, supervision, resources, and writing–review and editing. **Chun Feng:** Software and writing–review and editing. **Peng Wang:** Investigation and data curation. **Xiaolei Yue:** Investigation and data curation. **Tiejun Tao:** Investigation and data curation.

DATA AVAILABILITY STATEMENT

The data that support the findings of this study are available from the corresponding author upon reasonable request.

NOMENCLATURE

c_t	stress optical constant
d	denote the specimen thickness
$D_{T,L}$	maximum diameters of a caustics pattern
E	Young's modulus
$f(v)$	dynamic correction factor
G	shear modulus
G_f^I	mode I fracture energy
G_f^{II}	mode II fracture energy
K_I	mode I stress intensity factors
K_{II}	mode II stress intensity factors
k_n	normal stiffness
k_s	shear stiffness
SIFs	stress intensity factors
Z_0	distance between specimen middle plane and camera imaging plane
$\delta_{T,L}$	coefficient related to $D_{T,L}$
λ	scaled factor
μ	coefficient related to $(D_{L\max} - D_{L\min})/D_{L\max}$
ν	Poisson's rate
ρ	density
σ_T	normal stress in current time step
$\overline{\sigma}_T$	tensile strength of the host materials
σ_S	shear stress in current time step
$\overline{\sigma}_{TI}$	tensile strength of the interface
$\overline{\sigma}_{SI}$	tensile and shear strength of the interface

ORCID

Jun Zhou https://orcid.org/0000-0001-9180-3105

REFERENCES

1. Shi X, Yao W, Liu D, Xia K, Tang T, Shi Y. Experimental study of the dynamic fracture toughness of anisotropic black shale using notched semi-circular bend specimens. *Eng Fract Mech*. 2018;205:136-151.
2. Wu H, Pollard DD. Modeling a fracture set in a layered brittle material. *Eng Fract Mech*. 1992;42(6):1011-1017.
3. Wu J. Calculation of mixed-mode stress intensity factors for a crack normal to a bimaterial interface using contour integrals. *Eng Fract Mech*. 2003;70(13):1675-1695.
4. Gao Y, Feng XT. Study on damage evolution of intact and jointed marble subjected to cyclic true triaxial loading. *Eng Fract Mech*. 2019;215:224-234.
5. Ssa B, Edh B, Tk B, Hmn B. The effect of stress distribution on the shape and direction of hydraulic fractures in layered media. *Eng Fract Mech*. 2019;215:151-163.
6. Zuo JP, Li YL, Liu C, Liu HY, Lei L. Meso-fracture mechanism and its fracture toughness analysis of Longmaxi shale including different angles by means of M-SENB tests. *Eng Fract Mech*. 2019;215:178-192.
7. Wang J, Xie L, Xie H, et al. Effect of layer orientation on acoustic emission characteristics of anisotropic shale in Brazilian tests. *J Nat Gas Sci Eng*. 2016;36(Part B):1120-1129.
8. Heng S, Guo Y, Yang C, Daemen JJK, Li Z. Experimental and theoretical study of the anisotropic properties of shale. *Int J Rock Mech Min Sci*. 2015;74:58-68.
9. Ma T, Wu B, Fu J, Zhang Q, Chen P. Fracture pressure prediction for layered formations with anisotropic rock strengths. *J Nat Gas Sci Eng*. 2017;38:485-503.
10. Chalivendra VB, Rosakis AJ. Interaction of dynamic mode-I cracks with inclined interfaces. *Eng Fract Mech*. 2008;75(8):2385-2397.
11. Liu H, Meng X, Zhang H, Nie H, Li Y. The dynamic crack propagation behavior of mode I interlaminar crack in unidirectional carbon/epoxy composites. *Eng Fract Mech*. 2019;215:65-82.
12. Fei Y, Feng XT, Rong C, Xia K, Jin C. Dynamic tensile failure of the rock interface between tuff and basalt. *Rock Mech Rock Eng*. 2012;45(3):341-348.
13. Sundaram BM, Tippur HV. Dynamic crack growth normal to an interface in bi-layered materials: an experimental study using digital gradient sensing technique. *Exper Mech*. 2016;56(1):37-57.
14. Alneasan M, Behnia M, Bagherpour R. Analytical investigations of interface crack growth between two dissimilar rock layers under compression and tension. *Eng Geol*. 2019;259:1-12.
15. Qiu H, Zhu Z, Wang F, Wang M, Mao H. Dynamic behavior of a running crack crossing mortar-rock interface under impacting load. *Eng Fract Mech*. 2020;240:1-18.
16. Duan K, Kwok CY. Discrete element modeling of anisotropic rock under Brazilian test conditions. *Int J Rock Mech Min Sci*. 2015;78:46-56.
17. Dan DQ, Konietzky H, Herbst M. Brazilian tensile strength tests on some anisotropic rocks. *Int J Rock Mech Min Sci*. 2013;58:1-7.
18. Dan DQ, Konietzky H. Numerical simulations and interpretations of Brazilian tensile tests on transversely isotropic rocks. *Int J Rock Mech Min Sci*. 2014;71:53-63.
19. Tan X, Konietzky H, Frühwirt T, Dan DQ. Brazilian tests on transversely isotropic rocks: laboratory testing and numerical simulations. *Rock Mech Rock Eng*. 2015;48(4):1341-1351.
20. Qiu YZ, Yang R. Mode I stress intensity factors measurements in PMMA by caustics method: a comparison between low and high loading rate conditions. *Polym Test*. 2019;76:273-285.
21. Yue Z, Qiu P, Yang R, Zhang S, Yuan K, Li Z. Stress analysis of the interaction of a running crack and blasting waves by caustics method. *Eng Fract Mech*. 2017;184:339-351.
22. Yao XF, Xu W, Yeh HY. Investigation of crack tip evolution in functionally graded materials using optical caustics. *Polym Test*. 2007;26(1):122-131.
23. Yao XF, Xu W. Recent application of caustics on experimental dynamic fracture studies. *Fatigue Fract Eng Mater Struct*. 2011;34(6):448-459.
24. Sanford RJ. Determining fracture parameters with full-field optical methods. *Exper Mech*. 1989;29(3):241-247.
25. Zhou YY, Feng XT, Xu DP, Fan QX. An enhanced equivalent continuum model for layered rock mass incorporating bedding structure and stress dependence. *Int J Rock Mech Min Sci*. 2017;97:75-98.
26. Bouhala L, Shao Q, Koutsawa Y, et al. An XFEM crack-tip enrichment for a crack terminating at a bi-material interface. *Eng Fract Mech*. 2013;102:51-64.
27. Yang SQ, Yin PF, Huang YH. Experiment and discrete element modelling on strength, deformation and failure behaviour of shale under Brazilian compression. *Rock Mech Rock Eng*. 2019;52(7):4339-4359.
28. Liu Z, Xu H, Zhao Z, Chen Z. DEM modeling of interaction between the propagating fracture and multiple pre-existing cemented discontinuities in shale. *Rock Mech Rock Eng*. 2019;52(6):1993-2001.
29. Park B, Min KB. Bonded-particle discrete element modeling of mechanical behavior of transversely isotropic rock. *Int J Rock Mech Min Sci*. 2015;76:243-255.
30. Xiao HT, Yue ZQ. A three-dimensional displacement discontinuity method for crack problems in layered rocks. *Int J Rock Mech Min Sci*. 2011;48(3):412-420.
31. Wang XE, Yang J, Pan ZF, Wang FL, Meng YR, Zhu YH. Exploratory investigation into the post-fracture model of laminated tempered glass using combined Voronoi-FDEM approach. *Int J Mech Sci*. 2021;190:1-11.
32. Lisjak A, Garitte B, Grasselli G, Müller HR, Vietor T. The excavation of a circular tunnel in a bedded argillaceous rock (Opalinus clay): short-term rock mass response and FDEM numerical analysis. *Tunn Undergr Space Technol*. 2015;45(45):227-248.
33. Sun L, Liu Q, Grasselli G, Tang X. Simulation of thermal cracking in anisotropic shale formations using the combined finite-discrete element method. *Comput Geotech*. 2020;117:1-14.
34. Chen X, Chan A. Modelling impact fracture and fragmentation of laminated glass using the combined finite-discrete element method. *Int J Impact Eng*. 2018;112:15-29.
35. Ju Y, Wang Y, Su C, Zhang D, Ren Z. Numerical analysis of the dynamic evolution of mining-induced stresses and fractures in multilayered rock strata using continuum-based discrete element methods. *Int J Rock Mech Min Sci*. 2018;113:191-210.
36. Torabi AR, Pirhadi E. Notch failure in laminated composites under opening mode: the virtual isotropic material concept. *Composites*. 2019;172(SEP.1):61-75.

37. Torabi AR, Pirhadi E. Failure analysis of round-tip V-notched laminated composite plates under mixed mode I/II loading. *Theoret Appl Fract Mech*. 2019;104(2):1-16.
38. Alfano G, Crisfield MA. Finite element interface models for the delamination analysis of laminated composites: mechanical and computational issues. *Int J Numer Methods Eng*. 2001; 50(7):1701-1736.
39. Torabi AR, Pirhadi E. Extension of the virtual isotropic material concept to mixed mode I/II loading for predicting the last-ply-failure of U-notched glass/epoxy laminated composite specimens. *Compos Part B Eng*. 2019;176:1-12.
40. Song JH, Kim DJ, Lee SH, et al. A comparative study on dynamic fracture with finite element methods. *Computat Mech*. 2008;42(2):239-250.
41. Maio UD, Greco F, Leonetti L, et al. A refined diffuse cohesive approach for the failure analysis in quasibrittle materials—part I: theoretical formulation and numerical calibration. *Fatigue Fract Eng Mater Struct*. 2019;43(2):1-21.
42. Wang M, Gao K, Feng YT. An improved continuum-based finite–discrete element method with intra-element fracturing algorithm. *Comput Methods Appl Mech Eng*. 2021;384:1-17.
43. Torabi AR, Pirhadi E. On the ability of the notch fracture mechanics in predicting the last-ply-failure of blunt V-notched laminated composite specimens: a hard problem can be easily solved by conventional methods. *Eng Fract Mech*. 2019; 217:1-15.
44. Hao W, Sheng X, Guo G, Chen X, Zhu J. Mixed mode dynamic crack-fiber bundle interaction using caustics. *Polym Test*. 2016; 55:230-237.
45. Xu C, Yuan Y, Zhao C, Tan PJ, Xu X, Li Y. Dynamic crack-interface interactions in SGP laminated glass: an experimental investigation. *Mech Mater*. 2018;122:76-84.
46. Stein N, Weißgraeber P, Becker W. A model for brittle failure in adhesive lap joints of arbitrary joint configuration. *Compos Struct*. 2015;133:707-718.
47. Qiu P, Yue Z, Yang R, Ju Y. Modified mixed-mode caustics interpretation to study a running crack subjected to obliquely incident blast stress waves. *Int J Impact Eng*. 2021;150(3):1-19.
48. Theocaris PS. *Elastic Stress Intensity Factors Evaluated by Caustics*. Netherlands: Springer; 1981.
49. Ma K, Tang CA, Wang LX, et al. Stability analysis of underground oil storage caverns by an integrated numerical and microseismic monitoring approach. *Tunn Undergr Space Technol*. 2016;54:81-91.
50. Yue Z, Zhou J, Feng C, Li A, Qiu P, Gang M. Numerical investigation of the effect of holes on dynamic fracturing in multi-flawed granite. *Fatigue Fract Eng Mater Struct*. 2021; 44(7):1883-1896.
51. Besant T, Davies G, Hitchings D. Finite element modelling of low velocity impact of composite sandwich panels. *Composites Part a Applied Science and Manufacturing*. 2001; 32(9):1189-1196.
52. Gui Y, Bui HH, Kodikara J. An application of a cohesive fracture model combining compression, tension and shear in soft rocks. *Comput Geotech*. 2015;66(MAY):142-157.
53. Yue ZW, Zhou J, Chun F, Wang X, Linzhi P, Cong JY. Coupling of material point and continuum discontinuum element methods for simulating blast-induced fractures in rock. *Comput Geotech*. 2022;144:1-11.
54. Meng, Zhu, Zheming, et al. Study of the effect of empty holes on propagating cracks under blasting loads. *Int J Rock Mech Min Sci*. 2018;103:186-194.
55. Wang PD, Lei HS, Zhu XL, Chen HS, Fang DN. Investigation on the mechanical properties of epoxy resin with void defects using digital image correlation and image-based finite element method. *Polym Test*. 2018;72:223-231.

How to cite this article: Zhou J, Yue Z, Feng C, Wang P, Yue X, Tao T. Experiments and numerical simulations on dynamic crack behavior at the interface of layered brittle material. *Fatigue Fract Eng Mater Struct*. 2022;45(12):3546-3558. doi:10.1111/ffe.13829